Journal of Materials Chemistry B

Materials for biology and medicine

rsc.li/materials-b

Indexed in Medline!

ROYAL SOCIETY OF CHEMISTRY
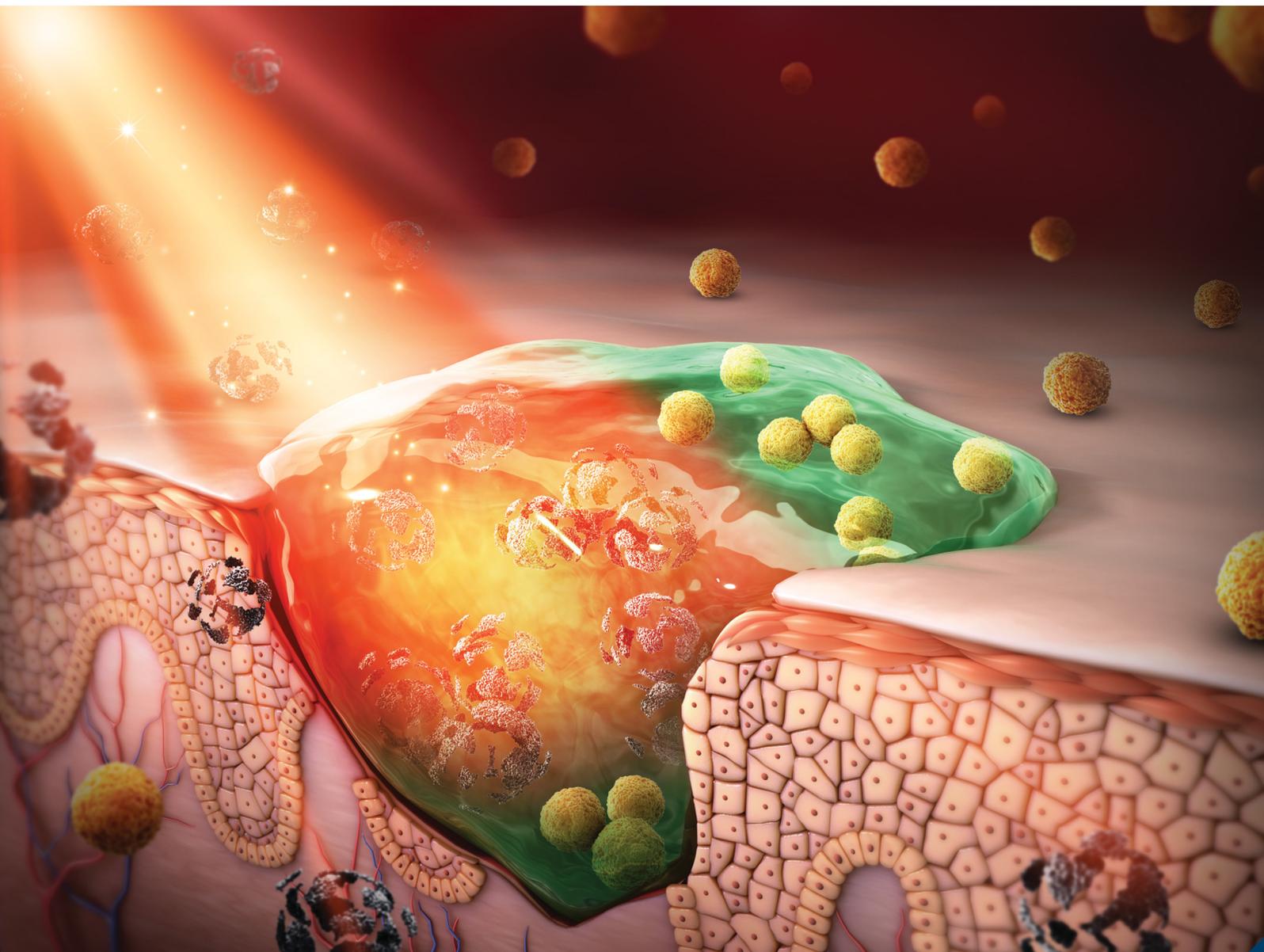
COMMUNICATION
Zhenhuan Jiang, Miao Wang, Guoqing Pan *et al.*
A dynamic nano-coordination protein hydrogel for
photothermal treatment and repair of infected skin injury

ROYAL SOCIETY
OF CHEMISTRY

COMMUNICATION

Check for updates

A dynamic nano-coordination protein hydrogel for photothermal treatment and repair of infected skin injury†

Weiling Yin,‡[a] Qiang Wang,‡[b] Jinyi Zhang,[a] Xu Chen,[a] Yunlong Wang,[a] Zhenhuan Jiang,*[b] Miao Wang*[a] and Guoqing Pan [iD] *[a]

In this work, a dynamic photothermal hydrogel based on copper disulfide nanoparticles and thiolated gelatin was reported. The resultant hydrogel enabled rapid photothermal sterilization and the sterilization rate could reach 99.9% after 10 minutes of near-infrared irradiation. In addition, the hydrogel exhibited typical dynamic properties with self-recovery, injectability and photothermal conversion ability, showing great potential as a highly adaptable and antibacterial wound dressing for infected tissue injuries.

Cutaneous wound infection represents one of the most ubiquitous and challenging matters in the clinic.[1] Protective dressings (fibrous membranes or hydrogels) with antibiotics or other antibacterial drugs are conventional means to treat skin infection.[2] However, these wound dressings are often enslaved to unbalanced protection (*i.e.*, low adaptability to wound geometry), especially when it involves drug-resistant bacterial infections.[3] Once the protective functions and antibacterial effects of wound dressings are lost (*e.g.*, external mechanical damage and drug-resistant bacteria), the infected injuries may develop into unhealing chronic wounds and even threaten life (*e.g.*, bone infections or limb amputation).[2c,4] Therefore, ideal skin wound dressings should be able to resist mechanical damage, adapt the wound geometry, and defeat drug-resistant bacteria, thus providing comprehensive protection and accelerating the repair of infected skin injuries.

Compared to conventional "static" materials in wound dressing fabrication, hydrogels with a reversibly crosslinked network show better adaptability in wound protection because of their dynamic properties.[1b,5] Dynamic hydrogels are capable of resisting external mechanical irritation and adapting amorphous wound geometries, thus showing potential as dressing materials with improved wound protection. In addition to physical protective function, advanced dressings should also have broad-spectrum bactericidal activity. Previously, the first choice for infections was chemotherapy. However, bacterial drug resistance, caused by the abuse of antibiotics or bactericidal substitutions, has now become a tough problem in the clinic.[3b] In contrast, physiotherapy is much safer.[1c,3c,6] We know since antiquity that heat treatment is an effective way to kill bacteria and even drug-resistant strains. More importantly, it will not induce drug resistance. Based on the above considerations, we anticipate that dynamic hydrogels with self-heating function would be a class of safe and effective wound protective materials for the treatment of infected tissue injuries.

Copper disulfide nanoparticles (CuS₂ NPs) are a type of semiconductor material with a suitable band gap capable of responding to near-infrared (NIR) excitation and producing photothermal effect.[7] CuS₂ NPs have attracted extensive attention in the biomedical field, especially in the fields of photothermal antibacterials,[8] photothermal cancer therapy,[9] *etc.* In addition, the potential of copper ions in coordination with different kinds of ligands exhibits the possibility to fabricate dynamic hydrogels with coordination-crosslinked networks. In this work, we report a protein-based, photothermal nanoparticle-coordinated, dynamic hydrogel based on CuS₂ as a multifunctional wound dressing for the treatment of infected skin wounds (Scheme 1). The dynamic nano-coordination protein hydrogel was prepared by facile combination of thiolated gelatin (SH-Gel) and photothermal conversion of CuS₂ NPs through reversible S–Cu coordination (Scheme 1A). Due to the reversible nature of the coordination,[10] the hydrogel exhibited dynamic properties like injectability and self-healing ability (Scheme 1B). Together with the photothermal effect of CuS₂ NPs,[7] we demonstrated that the dynamic hydrogel could be

[a] *Institute for Advanced Materials, School of Materials Science and Engineering, Jiangsu University, 301 Xuefu Road, Zhenjiang, Jiangsu, 212013, China.*
E-mail: wangmiao@ujs.edu.cn, panguoqing@ujs.edu.cn

[b] *Department of Orthopedics, People's Hospital of Yixing City, the Affiliated Yixing Hospital of Jiangsu University, Yixing, Jiangsu, 214200, P. R. China.*
E-mail: jiangzh1018@126.com

† Electronic supplementary information (ESI) available. See DOI: **https://doi.org/10.1039/d2tb01146h**

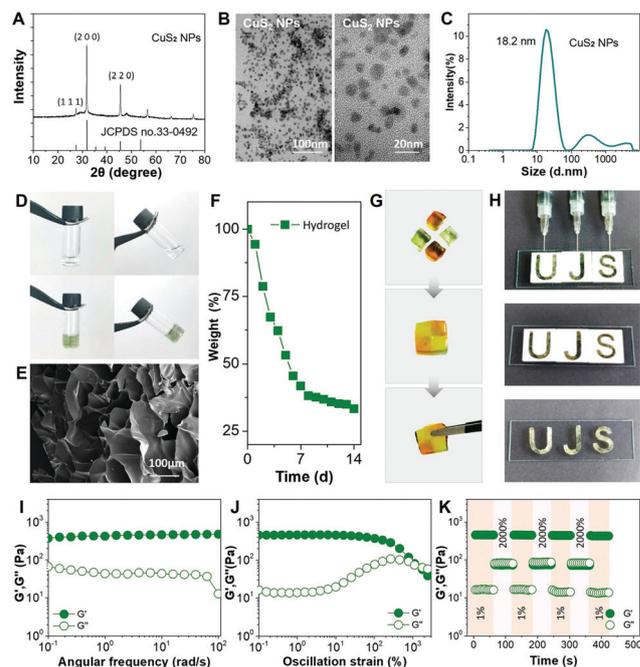‡ These authors contributed equally to this work.
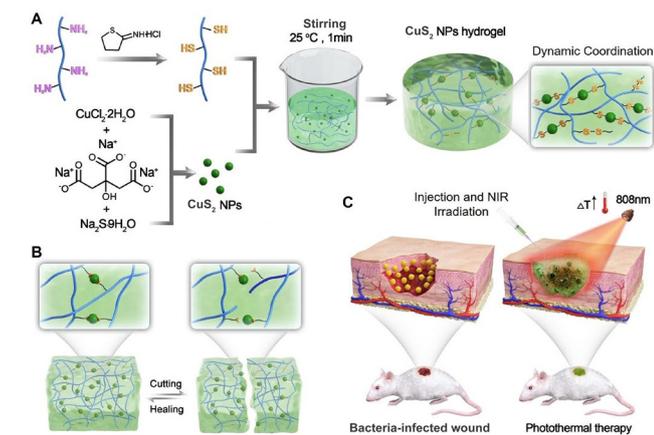
Scheme 1 Schematic illustration of the preparation of dynamic nano-coordination protein hydrogel and its application in infected skin tissue repair.

Fig. 1 Characterizations of CuS_2 NPs and the dynamic hydrogel. (A) XRD spectrum, (B) the TEM images, and (C) size distribution of CuS_2 NPs. (D) The gelation of the SH-Gel solution after addition of CuS_2 NPs. (E) SEM of the hydrogel. (F) *In vitro* degradation of the hydrogel. (G) Self-healing process of hydrogel blocks. (H) Injectability and remolding process of the hydrogel. (I) Dynamic oscillatory frequency sweeps (strain = 1%), (J) strain amplitude sweeps (frequency = 1 rad s^{-1}), and (K) step-strain sweeps (strain = 1% or 2000%, frequency = 1 rad s^{-1}) of the dynamic hydrogel.

used as a highly adaptable and antibacterial wound dressing for comprehensive protection and photothermal therapy of infected skin wounds (Scheme 1C).

Gelatin (Gel) was chosen because it is an extracellular matrix (ECM)-derived protein existing abundantly in skin tissues. Thiolated gelatin (SH-Gel) was synthesized by modifying the amino group with Traut's reagent.[11] The degree of thiolation was determined to be 10 mM g^{-1} using Ellman's reagent. CuS_2 NPs were hydrothermally synthesized according to previously reported methods.[7b] The CuS_2 NPs were characterized by X-ray diffraction (XRD) and transmission electron microscopy (TEM). The XRD pattern matched with the cubic CuS_2 phase (JCPDS No. 33-0492) (Fig. 1A). The TEM images showed that the NPs were relatively homogeneous and small at the nanoscale (∼18 nm) (Fig. 1B and C), which will facilitate the formation of more coordination interactions with SH-Gel at the nano-interfaces. As shown in Fig. 1D, the SH-Gel in solution was in a sol state without CuS_2 NPs. Upon the addition of CuS_2 NPs into the SH-Gel solution, a gelation process immediately occurred, leading to a light green hydrogel. The scanning electron microscopy (SEM) images revealed that the lyophilized hydrogel possessed a porous structure (Fig. 1E). The hydrogel also exhibited a moderate degradation period (Fig. 1F). The results confirmed the crosslinking between the CuS_2 NPs and SH-Gel. In view of the reversible nature of Cu–S coordination, we then investigated the dynamic properties of this hydrogel, *i.e.*, self-healing ability and injectability.[1b,12]

The hydrogel was first applied for a self-healing test. The blocks of hydrogel were stained with methyl orange and then contacted with each other for healing. As shown in Fig. 1G, the blocks showed rapid fusion at the contact interfaces within 10 minutes, and no obvious cracks were observed. In addition, the hydrogel also possessed shear thinning behaviour, *i.e.*, injectability. As shown in Fig. S1 (ESI†), the hydrogel could be easily squeezed out from the needle (22G) without obvious fracture. Using a letter-patterned mould, the hydrogel could be injected and shaped into intact letters (Fig. 1H). The results

verified that the hydrogel possessed typical dynamic characteristics, such as self-healing ability, injectability and moldability.

To further study the dynamism, rheology tests were performed.[5b] A dynamic oscillatory frequency sweep from 0.1 to 100 rad s^{-1} was first recorded (Fig. 1I). The hydrogel showed higher storage modulus (G') than loss modulus (G''), indicating a typical viscoelastic behaviour.[12] The relatively stable values of G' and G'' within the sweep indicated that the dynamic Cu–S coordination could effectively restrict the gelatin polymer chain motion. Strain sweep was then applied to evaluate the critical strain value in the case of hydrogel network damage. As shown in Fig. 1J, G'' of the hydrogel could keep at a higher level than G' under low strain, while the reverse was found when the strain increased over 1400%. This phenomenon suggested that the nano-coordination crosslinked network could resist against moderate mechanical agitation, but an enhanced agitation would lead to the breakage of the crosslinked network and collapse of the hydrogel, thus showing a state transition from gel to sol. The self-recovery property was finally examined by step-strain sweep by applying alternate strains (Fig. 1K). As shown, high oscillation excitation (2000% stain) resulted in the collapse of the coordination-crosslinked network, but it recovered immediately when the oscillation was relaxed. Moreover, G' and G'' could recover to their original values after repeated step-strain sweeps. The above rheology results well revealed the reversible molecular mechanism of the nano-coordination
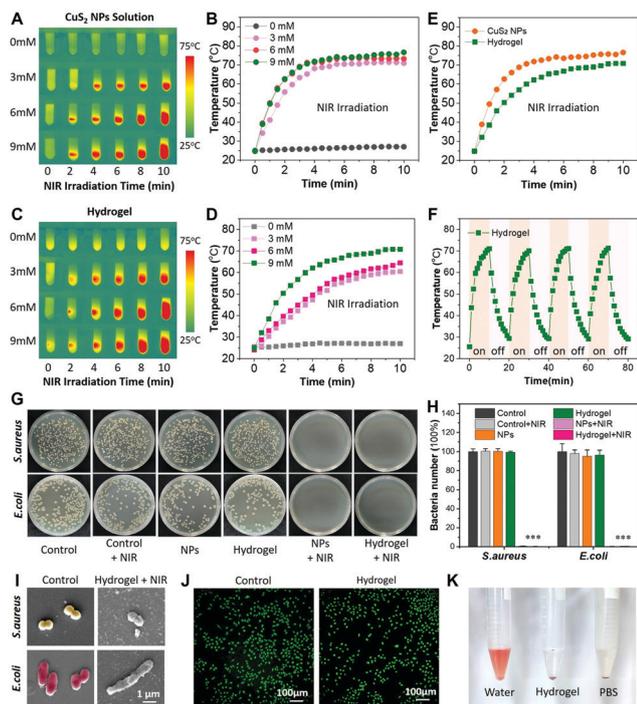
Fig. 2 Photothermal conversion effect and *in vitro* antibacterial activity. (A and C) Infrared thermal images and (B and D) temperature changes of CuS_2 NPs and hydrogels under NIR irradiation (808 nm, 2 w cm^{-2}), respectively. (E) Comparison of the photothermal conversion effects between the CuS_2 NP solution and the hydrogel. (F) Temperature changes of the hydrogel under on/off NIR irradiation. (G) Photos of agar plates with bacteria after different treatments. (H) *In vitro* antibacterial efficiency. (I) The SEM images of bacteria after treatment. (J) Live/dead cell-staining (L929) after incubation with the hydrogel. (K) Hemolysis of the hydrogel. Statistically significant differences are indicated by ***p < 0.001 as compared with others.
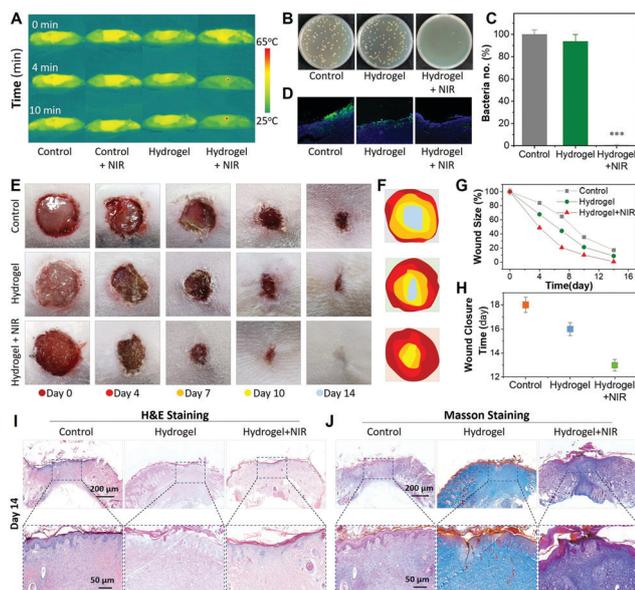
hydrogel. We believe that the dynamic property to resist mechanical damage would be a great virtue when this hydrogel is used as a skin wound dressing.

With the dynamic hydrogel in hand, we then investigated the photothermal responsiveness and antibacterial ability. Copper chalcogenides were widely reported as photothermal reagents, due to the strong absorption in the near-infrared (NIR) region.[7a] Thus, the photothermal conversion property of the CuS_2 NPs was first studied. Real-time temperature detection of different CuS_2 NP solutions was carried out using an infrared thermometer (an 808 nm NIR laser). As shown in Fig. 2A and B, after 10 min of NIR irradiation (2 w cm^{-2}), the temperature of the CuS_2 solution with concentrations at 3, 6 and 9 mM could increase from room temperature to 70.9, 73.6 and 76.7 °C, respectively. In contrast, the control solution without CuS_2 NPs showed a negligible temperature change. Likewise, the dynamic hydrogel exhibited similar photothermal responsiveness. Hydrogels with different concentrations all showed significant temperature increase after 2 min of NIR irradiation (Fig. 2C). We found that the NIR photothermal effects of CuS_2 NPs and the dynamic hydrogel were concentration-dependent and laser power intensity-dependent (Fig. 2B, D and Fig. S2, ESI†).

Increased concentration or enhanced laser power led to faster heating-up under NIR irradiation. Note that the photothermal conversion efficiency of the dynamic hydrogel showed a slightly lower efficiency than that of CuS_2 NPs. Nevertheless, the highest temperature of the hydrogel still could reach up to 70 °C (Fig. 2E). This temperature has proven to be enough to kill bacteria according to previous reported photothermal nanomaterials.[1c] Therefore, hydrogel with 9 mM CuS_2 NPs was chosen for the following studies. It is also worth mentioning that the photothermal effect of the hydrogel could be remotely controlled *via* NIR on/off switching. After four cycles of on-off irradiation, the photothermal effect and the dynamic hydrogel did not show obvious changes (Fig. 2F). The results indicated the robust photo-stability of the dynamic hydrogel. The excellent NIR photothermal conversion effect and photo-stability are favourable for the following photothermal bacterial killing assay both *in vitro* and *in vivo*.

The *in vitro* antibacterial activity was preliminarily tested against Gram-positive *S. aureus* and Gram-negative *E. coli* (Fig. 2G and H). As clearly shown in the images of agar plates, bacteria treated with CuS_2 NPs (9mM) and the dynamic hydrogel both exhibited significant bactericidal effects after NIR irradiation. Note that we did not observe the bacteriostatic effect of Cu ions in the CuS_2 NPs and hydrogel groups without NIR irradiation. Without NIR irradiation, neither CuS_2 NP solution nor the hydrogel showed significant bacterial killing effects on *S. aureus* and *E. coli*, and the results had no difference as compared with that of the blank control group. SEM was further employed to observe the morphologies of bacteria before and after treatment. As shown in Fig. 2I, the bacteria showed normal spherical (*S. aureus*) or rod (*E. coli*) shapes without any treatment. In contrast, the surface morphology of *S. aureus* and *E. coli* showed noticeable changes and their cell walls were contracted and deformed in the hydrogel group treated with NIR.[13] Moreover, under the visual field of a microscope, only sporadic and deformed bacteria could be found, further confirming the efficient bacterial killing effect. In addition to photothermal antibacterial activity, the dynamic hydrogel also exhibited good biocompatibility. Cells (L929) cultured with the hydrogel could maintain high viability (99.9%) and almost no dead cells were observed in 24 hours (Fig. 2J and Fig. S3, ESI†). We also found that cells incubated with the dynamic hydrogels under short-term NIR irradiation (4 min) did not show significant cytotoxicity. This would be a good choice for use as an alternative to NIR to balance the antibacterial activity and cytotoxicity of NIR. A hemolysis test was also used to show the low cytotoxicity of the hydrogel (Fig. 2K).[14] In contrast to the hypotonic hemolysis in pure water, the blood sample treated with the dynamic hydrogel did not show any hemolysis. The excellent photothermal antibacterial activity and low cytotoxicity demonstrated the great potential of this dynamic hydrogel as a biocompatible material for infection-prone tissue protection and repair.

The dynamic hydrogel was then used as a photothermal antibacterial dressing for the treatment of full-thickness cutaneous wounds with *S. aureus*-infection on Sprague-Dawley (SD)

This journal is © The Royal Society of Chemistry 2022

J. Mater. Chem. B, 2022, **10**, 8181–8185 | **8183**

Fig. 3 *In vivo* studies. (A) The infrared thermal images of subcutaneously injected hydrogels. (B and C) Agar plates with the exudate from *S. aureus*-infected wounds and (D) *S. aureus* antibody (green)-stained wound tissues after different treatments. (E and F) Healing processes of *S. aureus*-infected wounds in the SD rat model. (G) Quantitative results of wound size changes and (H) wound closure time. (I and J) H&E and Masson staining at day 14. Statistically significant difference is indicated by ***$p < 0.001$ as compared with others.

rats.[15] The *in vivo* photothermal conversion function of the hydrogel was first tested. The hydrogel was injected into the subcutaneous tissue of the dorsum panniculus carnosus and then irradiated under an 808 nm NIR laser. As shown in Fig. 3A, the temperature on the back region of hydrogel-injected SD rats showed a significant increase within 4 min under NIR irradiation. It could reach up to 62.8 °C after 10 min of irradiation. In contrast, the hydrogel-injected groups without NIR irradiation and the control groups all showed a negligible temperature increase. Given this, the hydrogel was applied for the treatment of *S. aureus*-infected skin wounds. After that the exudate from the wound sites was collected and re-cultured on agar plates (Fig. 3B). Compared to bacteria-covered plates in the control groups, no bacteria colonies were observed in the hydrogel/NIR co-treated group. Quantitative analysis confirmed that 99.9% of inoculated bacteria could be killed (Fig. 3C). Skin sections of the injected region were further applied for immunofluorescence staining against *S. aureus* after treatment.[15] As shown in Fig. 3D, skin sections in the control and the hydrogel group without NIR irradiation showed strong green fluorescence (*i.e.*, *S. aureus*) underneath the epidermal layer. In contrast, the bacterial intensity in the hydrogel/NIR co-treated group was significantly reduced. The results indicated the possibility of this dynamic hydrogel to kill bacteria hidden deep in the skin tissue.

The healing process of infected wounds was recorded with a digital camera. Different from the inflammatory redness and purulent exudate in the control and hydrogel groups without

NIR irradiation, the hydrogel/NIR co-treated wound bed had no pyogenic phenomena and became smaller from day 4 (Fig. 3E and F). These results indicated that the infection was effectively suppressed and the tissue reconstruction process was accelerated. We found that the hydrogel/NIR co-treated wounds could heal within two weeks, while the healing ratio was less than 90% within the same period in control groups (Fig. 3G). The average wound closure time in the control groups was 16–18 days, which was significantly longer than that in the hydrogel/NIR group (13 days) (Fig. 3H). The results also indicated that efficient control of infection could improve the tissue healing process.

Skin tissue sections were also applied for haematoxylin and eosin (H&E) and Masson's trichrome staining.[15] As shown in Fig. 3I and Fig. S4 (ESI†), fewer inflammatory cells were observed in the hydrogel/NIR group than in the control groups at days 7 and 14. We also found that the hydrogel/NIR group showed relatively regular epithelium, more hair follicles and complete dermal tissue at day 14. Moreover, in the hydrogel/NIR group, collagen deposition was improved with denser collagen fibers and better arrangement (Fig. 3J and Fig. S5, ESI†). The H&E and Masson staining results indicated that the hydrogel could effectively inhibit the infection-induced inflammatory response, which facilitated the ECM remolding process and subsequently accelerated tissue repair. In addition to skin tissues, several representative organs including the liver, kidneys, heart, spleen and lungs were also histologically examined. As expected, no pathological abnormality or lesion was observed in the histological images (Fig. S6, ESI†), indicating the biosafety of the hydrogel as a wound dressing.

In summary, we designed a multifunctional hydrogel with injectability, self-healing and photothermal conversion ability. The hydrogel, as a skin wound dressing, could adapt to the geometry of the wound site, resist mechanical damage, and photothermally kill pathogenic bacteria to accelerate infected skin healing, showing great potential as a tissue protective material for the treatment of infected wounds.

Conflicts of interest

There are no conflicts to declare.

Notes and references

1 (*a*) A. J. Singer and R. A. F. Clark, *N. Engl. J. Med.*, 1999, **341**, 738–746; (*b*) H. Chen, R. Cheng, X. Zhao, Y. Zhang, A. Tam, Y. Yan, H. Shen, Y. S. Zhang, J. Qi, Y. Feng, L. Liu, G. Pan, W. Cui and L. Deng, *NPG Asia Mater.*, 2019, **11**, 3; (*c*) J. Li, X. Liu, L. Tan, Z. Cui, X. Yang, Y. Liang, Z. Li, S. Zhu, Y. Zheng, K. W. K. Yeung, X. Wang and S. Wu, *Nat. Commun.*, 2019, **10**, 4490; (*d*) P. Wu, D. Chen, H. Yang,

8184 | *J. Mater. Chem. B*, 2022, **10**, 8181–8185

This journal is © The Royal Society of Chemistry 2022

C. Lai, C. Xuan, Y. Chen and X. Shi, *Smart Mater. Med.*, 2021, **2**, 172–181.

2 (*a*) M. A. Mofazzal Jahromi, P. Sahandi Zangabad, S. M. Moosavi Basri, K. Sahandi Zangabad, A. Ghamarypour, A. R. Aref, M. Karimi and M. R. Hamblin, *Adv. Drug Delivery Rev.*, 2018, **123**, 33–64; (*b*) B. Jiang, J. C. Larson, P. W. Drapala, V. H. Pérez-Luna, J. J. Kang-Mieler and E. M. Brey, *J. Biomed. Mater. Res., Part B*, 2012, **100B**, 668–676; (*c*) D. Ganary, D. Elizabeth and P. Tania, *Adv. Wound Care*, 2016, **5**, 32–41.

3 (*a*) S. Das and A. B. Baker, *Front. Bioeng. Biotechnol.*, 2016, **4**, 00082; (*b*) Y. Qiao, J. He, W. Chen, Y. Yu, W. Li, Z. Du, T. Xie, Y. Ye, S. Y. Hua, D. Zhong, K. Yao and M. Zhou, *ACS Nano*, 2020, **14**, 3299–3315; (*c*) Y. Xi, J. Ge, M. Wang, M. Chen, W. Niu, W. Cheng, Y. Xue, C. Lin and B. Lei, *ACS Nano*, 2020, **14**, 2904–2916; (*d*) Y. Yang, Y. Liang, J. Chen, X. Duan and B. Guo, *Bioact. Mater.*, 2022, **8**, 341–354.

4 V. Falanga, *Lancet*, 2005, **366**, 1736–1743.

5 (*a*) X. Zhao, H. Wu, B. Guo, R. Dong, Y. Qiu and P. X. Ma, *Biomaterials*, 2017, **122**, 34–47; (*b*) Y. Ma, P. He, W. Xie, Q. Zhang, W. Yin, J. Pan, M. Wang, X. Zhao and G. Pan, *Research*, 2021, **2021**, 9565402; (*c*) L. Cheng, Z. Cai, T. Ye, X. Yu, Z. Chen, Y. Yan, J. Qi, L. Wang, Z. Liu, W. Cui and L. Deng, *Adv. Funct. Mater.*, 2020, **30**, 2001196.

6 L. Rosselle, A. R. Cantelmo, A. Barras, N. Skandrani, M. Pastore, D. Aydin, L. Chambre, R. Sanyal, A. Sanyal, R. Boukherroub and S. Szunerits, *Biomater. Sci.*, 2020, **8**, 5911–5919.

7 (*a*) Y. Zhao and C. Burda, *Energy Environ. Sci.*, 2012, **5**, 5564–5576; (*b*) K. Du, S. Zhao, J. Feng, X. Gao, K. Liu, X. Wang, M. Zhang, Y. Li, Y. Lu and H. Zhang, *J. Mater. Chem. B*, 2021, **9**, 7216–7228.

8 (*a*) X. Wang, L. Fan, L. Cheng, Y. Sun, X. Wang, X. Zhong, Q. Shi, F. Gong, Y. Yang and Y. Ma, *iScience*, 2020, **23**, 101281; (*b*) B. Tao, C. Lin, Y. Deng, Z. Yuan, X. Shen, M. Chen, Y. He, Z. Peng, Y. Hu and K. Cai, *J. Mater. Chem. B*, 2019, **7**, 2534–2548.

9 X. Zhang, J. Wu, G. R. Williams, Y. Yang, S. Niu, Q. Qian and L.-M. Zhu, *J. Colloid Interface Sci.*, 2019, **539**, 433–441.

10 Y. Ma, X. Tian, L. Liu, J. Pan and G. Pan, *Acc. Chem. Res.*, 2019, **52**, 1611–1622.

11 S. Kommareddy and M. Amiji, *Bioconjugate Chem.*, 2005, **16**, 1423–1432.

12 M. C. Roberts, M. C. Hanson, A. P. Massey, E. A. Karren and P. F. Kiser, *Adv. Mater.*, 2007, **19**, 2503–2507.

13 R. Wu, Y. Ma, J. Pan, S.-H. Lee, J. Liu, H. Zhu, R. Gu, K. J. Shea and G. Pan, *Biosens. Bioelectron.*, 2018, **101**, 52–59.

14 K. Amin and R.-M. Dannenfelser, *J. Pharm. Sci.*, 2006, **95**, 1173–1176.

15 W. He, J. Bai, X. Chen, D. Suo, S. Wang, Q. Guo, W. Yin, D. Geng, M. Wang, G. Pan, X. Zhao and B. Li, *Proc. Natl. Acad. Sci. U. S. A.*, 2022, **119**, e2117221119.